Computational Materials Science 55 (2012) 419–429

Contents lists available at SciVerse ScienceDirect

Computational Materials Science

journal homepage: www.elsevier.com/locate/commatsci

Simulation of channel segregation using a two-phase columnar solidification model – Part II: Mechanism and parameter study

J. Li [a,b], M. Wu [a,b,*], J. Hao [a], A. Kharicha [a], A. Ludwig [a]

[a] Simulation and Modeling of Metallurgical Processes, Dept. of Metallurgy, Univ. of Leoben, A-8700 Leoben, Austria
[b] Christian Doppler Lab for Advanced Simulation of Solidification and Melting, Dept. of Metallurgy, Univ. of Leoben, A-8700 Leoben, Austria

ARTICLE INFO

Article history:
Received 30 September 2011
Received in revised form 7 December 2011
Accepted 19 December 2011
Available online 10 January 2012

Keywords:
Macrosegregation
Channel
Columnar solidification
Multiphase flow

ABSTRACT

In Part II of this investigation the two-phase columnar solidification model, described in Part I, is applied to study channel segregation in a Sn–10 wt.% Pb benchmark. Channel segregation originates from the thermo-solutal convection and the flow perturbations. The onset of a flow perturbation and subsequent channel segregation was previously analyzed with a mushy zone Rayleigh number by Beckermann et al. [Worster, Ann. Rev. Fluid Mech. (1997); Beckermann et al., Metall. Mater. Trans. A (2000)]. The current study has justified the Rayleigh number as a qualitative indicator for characterizing the origin of segregation channels. Numerical parameter study has shown that an enhanced mushy zone Rayleigh number by increasing the secondary dendrite arm spacing and/or solutal expansion coefficient is prone to the formation of the channel segregation. Newly formed channels are sustained via growth under certain preferential conditions of the resulting flow-solidification interactions, which can be characterized by a flow-solidification interaction term, $\vec{u}_\ell \cdot \nabla c_\ell$. Depending on the flow direction, the sign of this term can be positive or negative. Channels occur only in the region where the flow-solidification interaction term is negative. With a negative flow-solidification interaction term the increase in flow velocity due to a flow perturbation suppresses the local solidification rate, promoting the growth of the channel. In return the growing channel strengthens the flow perturbation, and the flow-solidification interaction term becomes more negative; thus the channel continues to grow and becomes stable. The current model indicates that remelting is not a necessary condition for channel segregation.

1. Introduction

Channel segregates, e.g. A-segregates in large steel ingots and freckles in unidirectionally solidified castings, are the consequence of thermal–solutal convection and the resulting flow interaction with the solidifying mushy zone [1–6]. Due to the engineering significance of alloy quality and durability, the formation mechanism of channel segregates has been the central focus of much theoretical and experimental research for many decades [4–12]. As large-scale computational power continues to become more accessible and affordable, numerical studies have also become a significant contributor to the investigation of channel segregates in the last decade [3,12–17].

The formation of channel segregates in a casting is dependent on the flow conditions present during solidification. The initial formation of channel segregates is believed to be the result of convection instability in the mushy zone near the primary dendrite tips [6]. For an alloy with a partition coefficient less than one ($k < 1$), the interdendritic melt becomes enriched with solute elements, which causes a change in the local melt density. Thus, the density of the interdentric melt is a function of both concentration and temperature. Depending on the thermal and solutal expansion coefficients and the solidification direction, varying thermo-solutal convection patterns in the mushy zone can develop as shown in Fig. 1. In the majority of engineering casting situations convection usually occurs as in Fig. 1b–d.

According to Worster [7] the onset of convection instability and channel formation can be analyzed in terms of the mushy zone Rayleigh number R_a, defined as the ratio of the thermo-solutal buoyancy force to the opposing friction force associated with the mush permeability. Beckermann and co-workers [12] have extended the previous definition of R_a by incorporating a more precise consideration of the solidification kinetics and the variable permeability of the mush:

$$R_a(h) = \frac{((\rho_0 - \rho_\ell)/\rho_0)\vec{g}\bar{K}h}{\alpha\nu}. \quad (1)$$

In this expression the R_a number is a function of the position h in the mushy zone, where h measures the depth of the mush from the primary dendrite tip, shown in Fig. 1b. The α and ν are thermal

* Corresponding author at: Simulation and Modeling of Metallurgical Processes, Dept. of Metallurgy, Univ. of Leoben, A-8700 Leoben, Austria. Tel.: +43 3842 4023103; fax: +43 3842 4023102.

E-mail address: Menghuai.wu@unileoben.ac.at (M. Wu).

0927-0256/$ - see front matter © 2011 Elsevier B.V. All rights reserved.
doi:10.1016/j.commatsci.2011.12.021

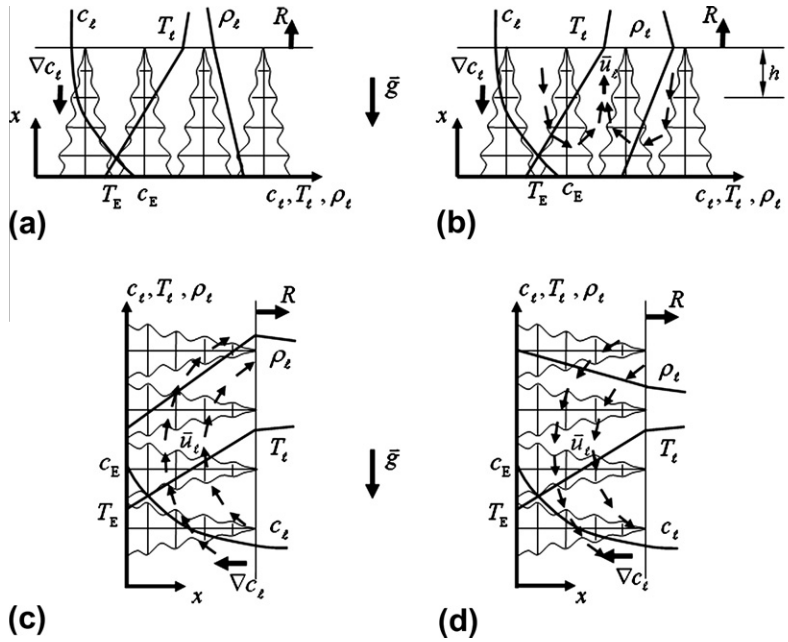

Fig. 1. Schematic of a solidifying mushy zone at a solidification velocity R. Toward the deep mushy zone, the temperature (T_ℓ) drops and the solute concentration (c_ℓ) increases, and the density of the interdendritic melt (ρ_ℓ) changes correspondingly. Depending on the thermal and solutal expansion coefficients and the direction of gravity $\overline{g}$, the following flow patterns may be induced: (a) no convection occurs in the case of the upward unidirectional solidification with the densest melt in the bottom of the mush; (b) in the case of the upward unidirectional solidification when the interdendritic melt becomes lighter toward the root of the mushy zone and convection cells are induced; (c) in the case of the lateral solidification with the densest melt near the solidification front, a clockwise convection pattern occurs; (d) in the case of the lateral solidification with the densest melt in the deep mushy zone, an anti-clockwise convection pattern occurs.

diffusivity and kinematic viscosity, ρ_0 is the reference density corresponding to the liquidus temperature and $\overline{K}$ is the mean permeability. It was found that if the maximum R_a in the mushy zone exceeded a critical number, 0.25, freckles tend to form.

Given that R_a varies significantly with thermal parameters such as the temperature gradient G and the solidification velocity R, Beckermann's definition of the R_a criterion can also be approximated as

$$\frac{1}{R^{n'}G^{n''}} < \text{constant}, \tag{2}$$

where n' and n'' are 1/2 and 1/5, respectively. When the above condition is fulfilled, channel segregates will not form. Other experimental researchers have also proposed similar criteria, with varying exponents and constants. For example, in an NH_4Cl–H_2O system, the exponents n' and n'' were found to be 1 and 1 [11]; Pollock and Murphy suggested 1/2 and 1/4 for the Ni-based superalloys [18]; and Suzuki and Miyamoto used 2.1 and 1 for large steel ingots [8,9]. As G and R are important, but not the only factors influencing channel segregation, the above discrepancy suggested further investigation as worthwhile.The onset of convection instability is not a sufficient condition to ensure the formation of channels; the channels must be stabilized by the resulting flow-solidification interaction. The coupling between the interdendritic flow and solidification is a key factor for channel growth. Solidification of the mushy zone can be accelerated at one location, or suppressed (even leading to remelting) at another location by the flow [4,5,12]. For the unidirectional solidification case in Fig. 1b, the segregated melt is lighter, tends to rise and induces a convection cell. The rising melt, bringing the segregated melt upwards, suppresses solidification and/or encourages localized remelting such that a pencil-like plume (chimney) forms, leading to the formation of freckles as observed in many super-alloy castings. For the lateral solidification cases of Fig. 1c and d, flow perturbation can occur at different positions (height). However, the flow perturbation can only create stable channels in some preferential regions. Meherabian and co-authors proposed an analytical correlation between the solidification rate and the flow velocity, $\vec{u}_\ell$, [4,5] based on Flemings' local solute redistribution equation [1],

$$\frac{\partial f_\ell}{\partial T} = -\left(\frac{1-\beta}{1-k}\cdot\frac{f_\ell}{c_\ell^*}\cdot\frac{\partial c_\ell^*}{\partial T}\right)\left(1+\frac{\vec{u}_\ell\cdot\overline{G}}{\dot{T}}\right). \tag{3}$$

Here $\beta = ((\rho_s - \rho_\ell)/\rho_s)$, the solidification shrinkage, and c_ℓ^* is the thermodynamic equilibrium concentration, assumed to be equal to the local melt concentration, c_ℓ. The sign of the first term in parenthesis on the right hand side of Eq. (3) is always negative regardless of k, and the sign of the cooling rate $\dot{T}$ is always negative. Therefore, the sign of $\partial f_\ell/\partial T$, determining the acceleration or suppression (even remelting) of solidification, depends on the sign and magnitude of the term $\vec{u}_\ell\cdot\overline{G}$. This analysis predicts that a stable channel will form when $\vec{u}_\ell\cdot\overline{G} > |\dot{T}|$, which causes $\partial f_\ell/\partial T$ to be

Table 1
Numerical parameter study by varying λ_2 and β_c.

Simulation case	λ_2 (μm)	β_c	$R_{a,Max}$ [a]	Channel or not
1	32.5	−1.06	0.02	No
2	65	−0.53	0.05	No
3	97.5	−0.53	0.11	No
4	65	−1.06	0.12	No
5	130	−0.53	0.24	Yes
6	97.5	−1.06	0.28	Yes
7	65	−2.65	0.32	Yes
8	65	−5.3	0.54	Yes
9	195	−0.53	0.68	Yes
10	260	−0.53	1.25	Yes
11	325	−0.53	2.05	Yes
12	455	−0.53	7.04	Yes
13	650	−0.53	13.22	Yes

[a] Maximum Rayleigh number ($R_{a,Max}$) being reached during the initial stage (10 s) of solidification.

negative. In other words, a sufficiently strong interdendritic flow in the direction of the temperature gradient will cause remelting of dendrites and an open channel will form. If $\vec{u}_\ell \cdot \vec{G} < 0$, i.e. flow is in the direction opposite to the temperature gradient and $\partial f_\ell / \partial T$ is positive, hence there is no possibility for stable channel to form. A third, intermediate case arises if $|\dot{T}| > \vec{u}_\ell \cdot \vec{G} > 0$, i.e. interdendritic flow is in the direction of temperature gradient and $\partial f_\ell / \partial T$ is still positive, but is reduced by the flow. In other words, solidification still proceeds with decreasing temperature, but the solidification rate is locally suppressed by the flow. In this intermediate case channels might form.

Eq. (3) can be applied to qualitatively analyze the potential formation of channel segregates. For example, in the lateral solidification case of Fig. 1c, the interdendritic melt, with a relatively higher concentration of solute element, is lighter and tends to rise and escape from the mushy zone in the upper part of the casting. The escaping melt suppresses solidification and may cause localized remelting, such that channels form, leading to the A-segregation observed in many steel ingots. Channels are not able to form in the bottom region in such a configuration. In the lateral solidification of Fig. 1d where the interdendritic melt is denser, channels form in the bottom region, as demonstrated in the current Sn–Pb benchmark (Part I).

Part II of this investigation examines the formation mechanism of channel segregates in the Sn–10 wt.% Pb benchmark using a two-phase columnar solidification model [19,20]. The current model differs from previous channel segregation models by including diffusion of the solute element in the interdendritic melt as a governing factor of solidification. Therefore, the significance of the diffusivity of the solute element is also discussed. An in-depth parameter study of the R_a number, by varying the mush permeability, is presented. The benchmark studied is similar to the lateral solidification case of Fig. 1d, however the conclusions from this study can be applied to the case of Fig. 1c.

2. Growth of channels

2.1. Flow-solidification interaction

After the initial formation, a channel may either continue to grow or disappear depending on the flow-solidification interaction in the two-phase mushy zone. Following the work of Meherabian and co-authors [4], a correlation of the local solidification rate ($M_{\ell c}$) to the flow velocity ($\vec{u}_\ell$) is established to better capture the phenomena of channel segregation in the situation of diffusion-governed solidification. The mass and species conservation equations for the two-phase columnar solidification model are summarized in Table 1 of Part I. A detailed description of the model is presented in the authors' previous publications [19,20]. The current model includes the following key assumptions [21]:

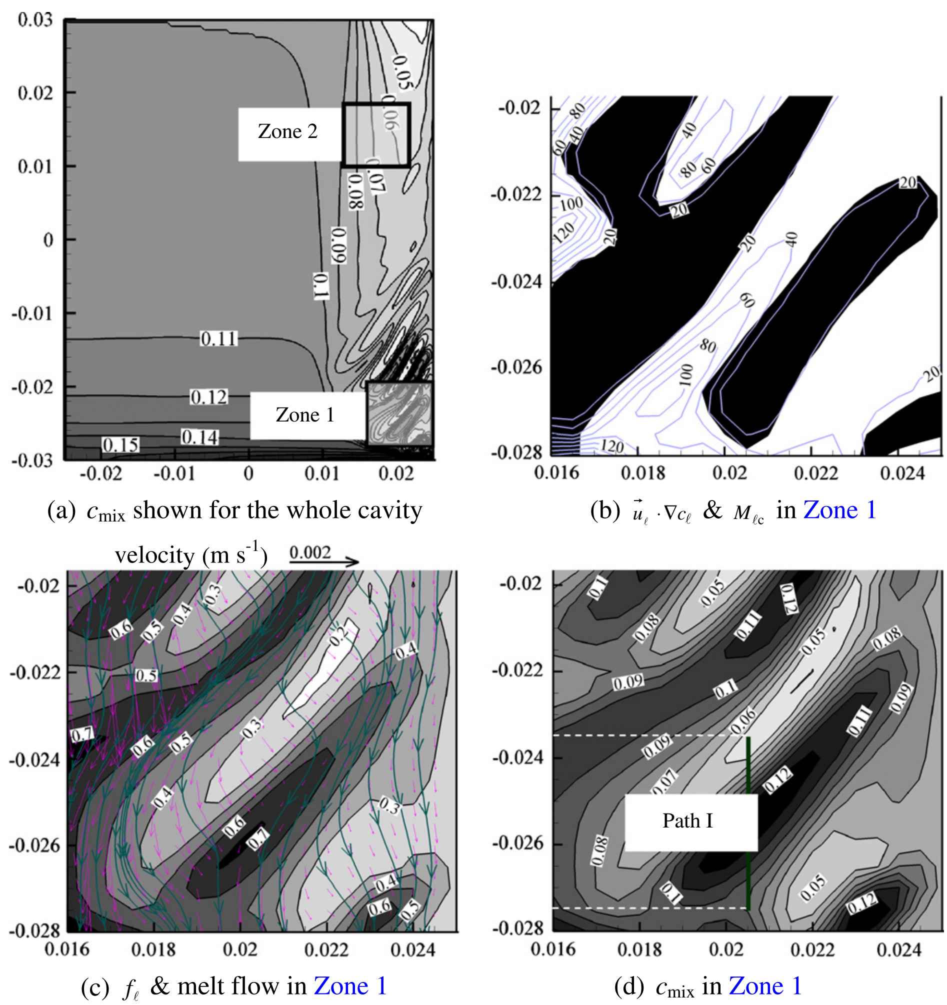

(a) c_{mix} shown for the whole cavity (b) $\vec{u}_\ell \cdot \nabla c_\ell$ & $M_{\ell c}$ in Zone 1 (c) f_ℓ & melt flow in Zone 1 (d) c_{mix} in Zone 1

Fig. 2. Analysis of the formation of the channel segregation at $t = 40$ s: (a) mixture concentration (c_{mix}) distribution in the cavity is shown in gray scale and isolines; (b) contours of the flow-solidification interaction term ($\overline{u}_\ell \cdot \nabla c_\ell$) in white (positive) and black (negative) overlaid by the mass transfer rate ($M_{\ell c}$) isolines; (c) liquid volume fraction (f_ℓ) contours and f_ℓ isolines overlaid by vectors of liquid velocity and streamlines; and (d) c_{mix} contour and its isolines.

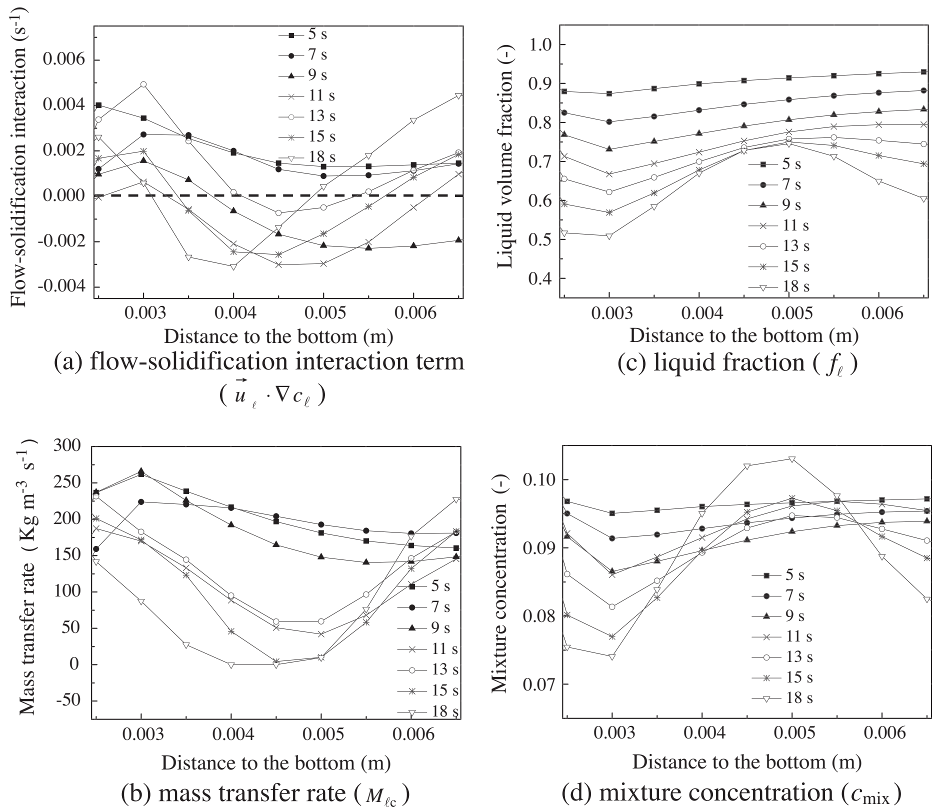

Fig. 3. Analysis of the evolution of channels and channel segregates along Path I as marked in Fig. 2d in terms of (a) $\vec{u}_\ell \cdot \nabla c_\ell$, (b) $M_{\ell c}$, (c) f_ℓ and (d) c_{mix}.

The flow is driven by thermo-solutal buoyancy. The solidification shrinkage is neglected, i.e., both solid and liquid have the same and constant density ($\rho_s = \rho_\ell = \rho$), with a Boussinesq approach used to treat thermo-solutal convection.
Solidification is modeled with a columnar dendritic morphology. The columnar dendrite is approximated by step-wise growing cylinders with constant (primary arm) spacing, and the growth rate of the columnar phase is governed by diffusion around the cylindrical trunk.
Species partitioning occurs at the liquid–solid interface, $\partial(f_s\rho_s c_s)/\partial t = c_s^* \rho_s \partial f_s/\partial t$, where c_ℓ^* and c_s^* are thermodynamic equilibrium concentrations at the liquid–solid interface.
At the macroscopic scale (global species transport) diffusion is neglected ($D_\ell = 0$, $D_s = 0$), while at the microscopic scale diffusion in the interdendritic melt is considered ($D_\ell \neq 0$) and back diffusion in the solid is ignored ($D_s = 0$).
The solidified phase is stationary: $\vec{u}_s = 0$.

The species conservation equation is written as

$$c_s^* \rho_s \frac{\partial f_s}{\partial t} + \rho_\ell c_\ell \frac{\partial f_\ell}{\partial t} + \rho_\ell f_\ell \frac{\partial c_\ell}{\partial t} + \nabla \cdot (f_\ell \rho_\ell c_\ell \bar{u}_\ell) = 0. \tag{4}$$

Substituting the mass conservation equation into Eq. (4) the time derivative of the liquid concentration is

$$\frac{\partial c_\ell}{\partial t} = -\frac{(c_\ell - c_s^*)}{f_\ell} \cdot \frac{\partial f_\ell}{\partial t} - \bar{u}_\ell \cdot \nabla c_\ell. \tag{5}$$

Taking the time derivative of $T = T_f + mc_\ell^*$, the changing liquid interface concentration is

$$\frac{\partial c_\ell^*}{\partial t} = \frac{1}{m} \frac{\partial T}{\partial t}. \tag{6}$$

Subtracting Eq. (5) from Eq. (6) results in the local rate of change of $(c_\ell^* - c_\ell)$

$$\frac{\partial (c_\ell^* - c_\ell)}{\partial t} = \frac{(c_\ell - c_s^*)}{f_\ell} \frac{\partial f_\ell}{\partial t} + \frac{1}{m} \frac{\partial T}{\partial t} + \vec{u}_\ell \cdot \nabla c_\ell. \tag{7}$$

In the left hand side (LHS) of Eq. (7), $(c_\ell^* - c_\ell)$ is the driving force for solidification/melting, which governs the solidification/melting rate, $M_{\ell c}$ [19–21].

The local solidification/melting rate is the result of three contributions, corresponding to the three right hand side (RHS) terms of Eq. (7). The first RHS term is the contribution of the solidification-induced solute enrichment of the interdendritic melt, the sign of which is always negative for solidification. The solidification rate decreases with solute enrichment of the interdendritic melt. The second RHS term is the contribution of the cooling rate, the sign of which is always positive, i.e., the solidification rate increases with enhanced cooling. These first two terms are relatively stable during solidification and are not considered critical factors in channel formation.The third RHS term in Eq. (7), $\bar{u}_\ell \cdot \nabla c_\ell$, is a flow-solidification interaction term, which is the most critical for the formation of the channel. Depending on the interdendritic flow, the sign of this term can be positive or negative. Local solidification behavior depends on the sign of the flow-solidification interaction term. In a region where the melt flows in the same direction as the concentration gradient, the flow-solidification interaction term is positive. The local increase in flow velocity due to a flow perturbation accelerates solidification and as a consequence of the locally accelerated solidification the flow permeability (K) becomes relatively smaller than that of neighboring zones and the interdentric flow slows down. In other words, the increase in flow velocity induced by a flow perturbation is throttled through the enhanced solidification. In the same sense, the local decrease in flow velocity due to a perturbation is reinforced by the decreased solidification rate. The region with a positive flow-solidification interaction term is an accelerated solidification region where flow perturbations are throttled through the flow-solidification interaction and channels do not form.

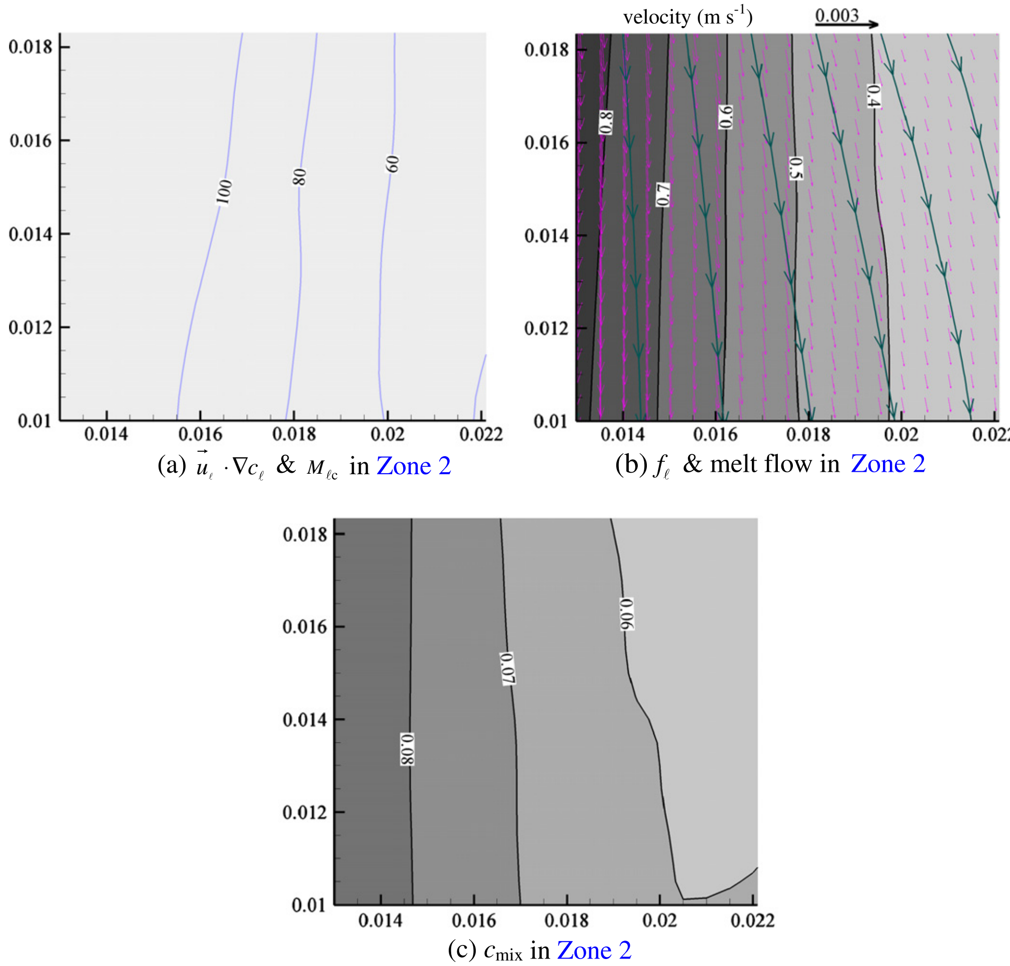

(a) $\vec{u}_\ell \cdot \nabla c_\ell$ & $M_{\ell c}$ in Zone 2

(b) f_ℓ & melt flow in Zone 2

(c) c_{mix} in Zone 2

Fig. 4. Analysis of the channel-free zone (Zone 2 of Fig. 2a) at $t = 40$ s. (a) contours of $\overline{u}_\ell \cdot \nabla c_\ell$ in white (positive) and black (negative) overlaid with $M_{\ell c}$ isolines, $\overline{u}_\ell \cdot \nabla c_\ell$ is positive everywhere; (b) f_ℓ contours and isolines overlaid by liquid velocity vectors and streamlines; (c) c_{mix} contours and isolines.

In regions where the melt flows in the opposite direction of the concentration gradient, the flow-solidification interaction term is negative. The local increase in flow velocity due to a flow perturbation suppresses the solidification rate. This region with a relatively lower solid fraction has a larger permeability and the flow becomes stronger. In other words, the local increase in flow velocity due to a flow perturbation is reinforced by the suppressed solidification. In the same sense, a local decrease in flow velocity due to a flow perturbation is further decreased by the increased solidification rate. As a consequence of the flow-solidification interaction, the magnitude of the initial flow perturbation is increased. The region with a negative flow-solidification interaction term is a suppressed solidification region where channels form.

The above hypothesis on channel formation is verified by the current modeling results, as detailed in Figs. 2–4. The results shown here are obtained from a 2D simulation of Sn–10 wt.% Pb benchmark (0.05×0.06 m^2). Heat is extracted from the vertical (right) wall, and solidification proceeds laterally from the right towards the plane of symmetry. The two-phase columnar solidification model, computational domain, material properties and process parameters, were described in Part I of this study.

At 40 s channels are observed in the right bottom region, as shown in Fig. 2a. The global flow pattern in the cavity is similar to the case of Fig. 1d, namely the solute enriched interdendritic melt is denser than the bulk melt. The interdendritic melt sinks in the mushy zone, causing a suppressed solidification zone in the lower region. A zoomed view shows the details of the channel formation in Zone 1 (near right bottom corner) in Fig. 2b–d. The suppressed solidification zones, corresponding to negative $\vec{u}_\ell \cdot \nabla c_\ell$, are shown in black in Fig. 2b. The solidification rate in the suppressed-solidification (black) zones is significantly decreased by the flow. The solidification (mass transfer) rate, $M_{\ell c}$, in these zones is relatively small, ~20 kg m^{-3} s^{-1}, in comparison with neighboring zones where $M_{\ell c}$ reaches as high as 120 kg m^{-3} s^{-1}. The change in solidification rate due to a flow perturbation leads to the growth of the channel. As soon as a channel forms, the flow takes the path of least resistance through the channel, in Fig. 2c, hence the flow streamlines are strongly influenced by the forming channels. Inside the channels the interdentric flow travels through the channel paths while in the immediate neighboring zones the flow is diverted almost vertically across the channel wall(s). The macrosegregation distribution (c_{mix}) in Fig. 2d has a similar distribution pattern to f_ℓ and the flow-solidification interaction term. Throughout the solidification process, the value of $M_{\ell c}$ stays positive-indicating that the mass is always transferred from the liquid to the solid phase, and channels form without evidence of remelting.

The dynamic evolution of the channel is further analyzed in Fig. 3 by tracking the flow-solidification interaction term ($\vec{u}_\ell \cdot \nabla c_\ell$), mass transfer rate ($M_{\ell c}$), liquid volume fraction (f_ℓ) and mixture concentration (c_{mix}) along a vertical path in the simulation domain. The path (Path I, as marked in Fig. 2d) crosses one channel, from 0.0025 m to 0.0065 m (distance from the bottom). The formation of the channel can be analyzed by f_ℓ and c_{mix} curves,

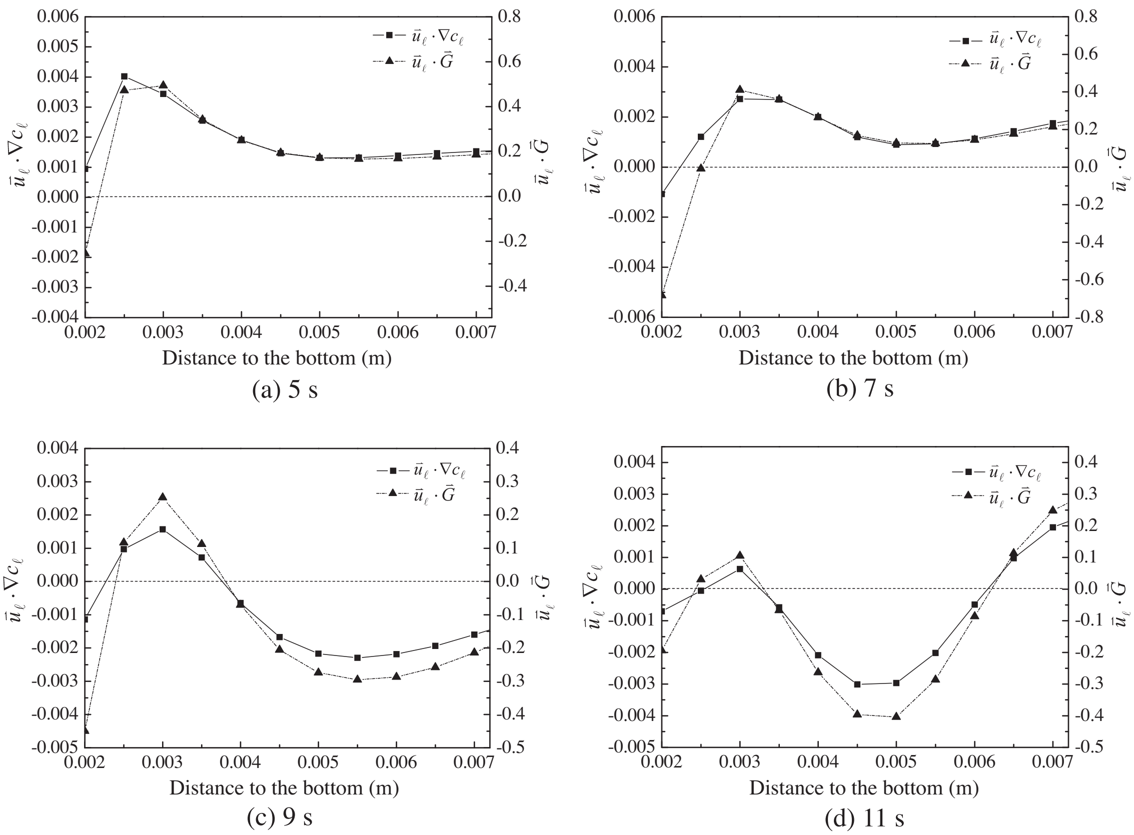

Fig. 5. Evolution of the flow-solidification interaction term, which is defined by $\vec{u}_\ell \cdot \nabla c_\ell$ and $\overline{u}_\ell \cdot \overline{G}$. The curves are plotted along the path I as marked in Fig. 2d. (a) 5 s; (b) 7 s; (c) 9 s; (d) 11 s.

when they become arched-upwards. Generally, the curves of $\vec{u}_\ell \cdot \nabla c_\ell$ are quite similar to the curves of $M_{\ell c}$, Fig. 3a and b, indicating a strong interaction between the flow and the mass transfer. This further verifies that among the three RHS terms of Eq. (7) the flow-solidification interaction term is the most critical in determining the variation of $M_{\ell c}$. If the flow-solidification interaction term is not negative (e.g. before 7 s), channels are not prone to form. At 9 s, the flow-solidification interaction term is negative in the upper section of Path I – solidification is suppressed leading to a reduction of $M_{\ell c}$. However, the arching of the f_ℓ curve, an indicator of channel formation, is not yet evident. Up to 13 s the flow-solidification interaction term stays locally negative in a somewhat oscillatory manner, the $M_{\ell c}$ curves become concave-downwards, and the onset of channel formation can be identified from the f_ℓ curve and c_{mix} curve. At 15 s in the suppressed solidification region $M_{\ell c}$ is only 9 kg m^{-3} s^{-1}, about 200 kg m^{-3} s^{-1} smaller than the neighboring regions. As the difference in solidification rate between the suppressed solidification area and neighboring regions becomes greater, the channel becomes larger and more stable. Again, during the entire solidification process, $M_{\ell c}$ is never negative-formation of the channel appears to be entirely due to the change in the solidification rate caused by flow instability.

As proof of the aforementioned hypothesis, that channels cannot form in the solidification-accelerated region, the solidification process in the accelerated solidification region is also examined, as shown in Fig. 4. The flow-solidification interaction term $\vec{u}_\ell \cdot \nabla c_\ell$ is positive everywhere in Zone 2. Any increase in flow due to local flow perturbations will be throttled by the accelerated solidification. The f_ℓ isolines and the flow streamlines are smooth and undisturbed, thus, channels do not appear in this region.

Recently, Sawada and co-authors [22] studied the mechanism of channel segregation in vertical directional solidification with a Pb–10 wt.% Sn alloy, and reported a similar conclusion regarding the accelerated and suppressed solidification zones.

2.2. Significance of the finite diffusion in the interdendritic melt

Eqs. (3) and (7) differ in the treatment of diffusion of the solute element in the interdentritc melt. Eq. (3) is derived on the assumption of infinite diffusion of the solute element in the interdendritic melt while Eq. (7) includes this diffusion. When an assumption of infinite diffusion in the interdendritic melt is applicable (i.e. $c_\ell = c_\ell^*$), one can use the definition of the flow-solidification interaction term $\vec{u}_\ell \cdot \overline{G}$ instead of $\vec{u}_\ell \cdot \nabla c_\ell$ to analyze channel formation. For many engineering cases of solidification, infinite diffusion in the interdendritic melt represents a reasonable approximation and the term $\overline{u}_\ell \cdot \overline{G}$ has been successfully used to analyze channel formation [4,5]. However, when the influence of the interdendritic diffusion is significant, an analysis based on the term $\overline{u}_\ell \cdot \nabla c_\ell$ is more reliable.

Fig. 5 shows the evolution of the flow-solidification term, which was defined in two ways, i.e. $\overline{u}_\ell \cdot \nabla c_\ell$ and $\overline{u}_\ell \cdot \overline{G}$, along the same path. As expected, the evolution of the $\overline{u}_\ell \cdot \overline{G}$ curves and $\overline{u}_\ell \cdot \nabla c_\ell$ curves show quite similar behavior. Small differences exist in the curves, particularly in the lower region of the benchmark, however the oscillation frequencies between the positive and negative values show the same trend. This indicates that the flow-solidification interaction term ($\vec{u}_\ell \cdot \overline{G}$), based on the infinite diffusion assumption, is a good approximation for a qualitative investigation on the formation of the channel segregation for the current bench-

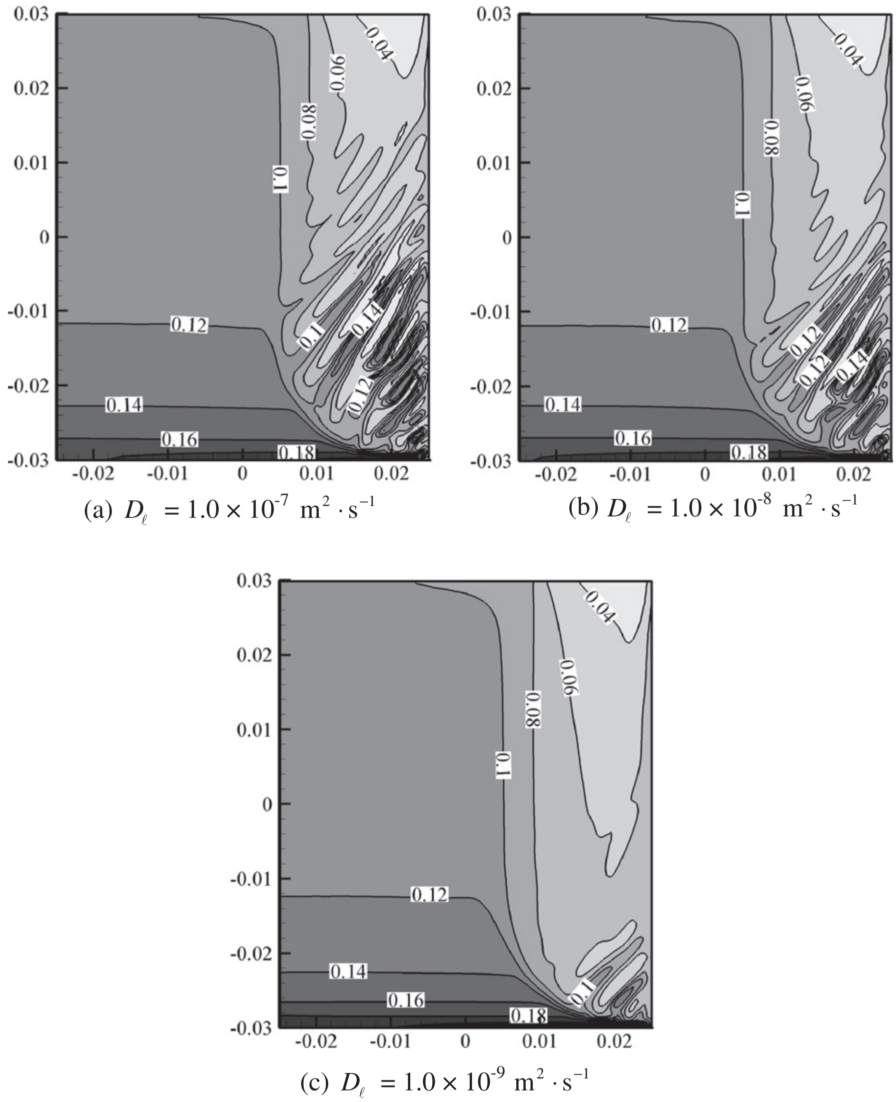

Fig. 6. Influence of the liquid diffusion coefficient D_ℓ on the channel segregation. Results at the moment 70 s are shown. c_{mix} map is overlaid with c_{mix}-isotherm. (a) $D_\ell = 1.0 \times 10^{-7}\ \mathrm{m^2\ s^{-1}}$; (b) $D_\ell = 1.0 \times 10^{-8}\ \mathrm{m^2\ s^{-1}}$; (c) $D_\ell = 1.0 \times 10^{-9}\ \mathrm{m^2\ s^{-1}}$.

mark.To verify the significance of solute diffusion in the interdendritic melt, further simulations were made by varying D_ℓ from (a) 1.0×10^{-7}, (b) 1.0×10^{-8}, (c) $1.0 \times 10^{-9}\ \mathrm{m^2\ s^{-1}}$. As shown in Fig. 6, the tendency for channel segregation to occur (the amount of channels, the area where the channels occur, and the severity of segregation) increases as D_ℓ increases. The case with $D_\ell = 1.0 \times 10^{-7}$ is closest to the assumption of infinite diffusion, where channel segregation is slightly overestimated. When the diffusivity is very small, 1.0×10^{-9}, channel formation is inhibited. This indicates that the validity of $\vec{u}_\ell \cdot \overline{G}$ for the investigation of channel formation is limited to alloys with large solute diffusivity in the interdendritic melt.

3. Onset of channels

3.1. Parameter study

As previously studied, the onset of channel formation can be characterized by the Rayleigh number [7,12], i.e. the ratio of the thermo-solutal buoyancy force to the friction force associated with mushy zone permeability. The mushy zone permeability is proportional to the square of secondary dendrite arm spacing, $K \propto \lambda_2^2$, and the key parameters for the buoyancy force are the expansion coefficients β_c and β_T.

Thus, the sensitivity of the channel segregation to Rayleigh number is investigated by varying λ_2 and β_c, as listed in Table 1. All other physical and process parameters are kept constant.

Figs. 7 and 8 compare the simulation results of four cases by varying λ_2. As λ_2 increases resistance to the interdendritic flow decreases and heat and mass transfer are enhanced. As shown by the isotherms in Fig. 7 the heat extraction in Case 13 (large λ_2) appears to be faster than that in Case 2 (small λ_2). At t = 150 s the temperature near the plane of symmetry of Case 13 is lower than that of Case 2, and the isotherms move slightly faster toward the plane of symmetry as λ_2 increases.

The influence of λ_2 on f_ℓ and c_{mix} is more evident than the influence of λ_2 on heat transfer. When λ_2 is small (<100 μm) the friction resistance of the dendrites is high enough to maintain a stable interdendritic liquid flow; channels and channel segregation are not observed, as shown in Figs. 7a and 8a. Channels and channel segregation occur only when λ_2 is sufficiently large ($\geqslant$260 μm), as shown in Figs. 7b–d and 8b–d. The number of the channels found in the calculation domain is dependent on λ_2. For λ_2 equal

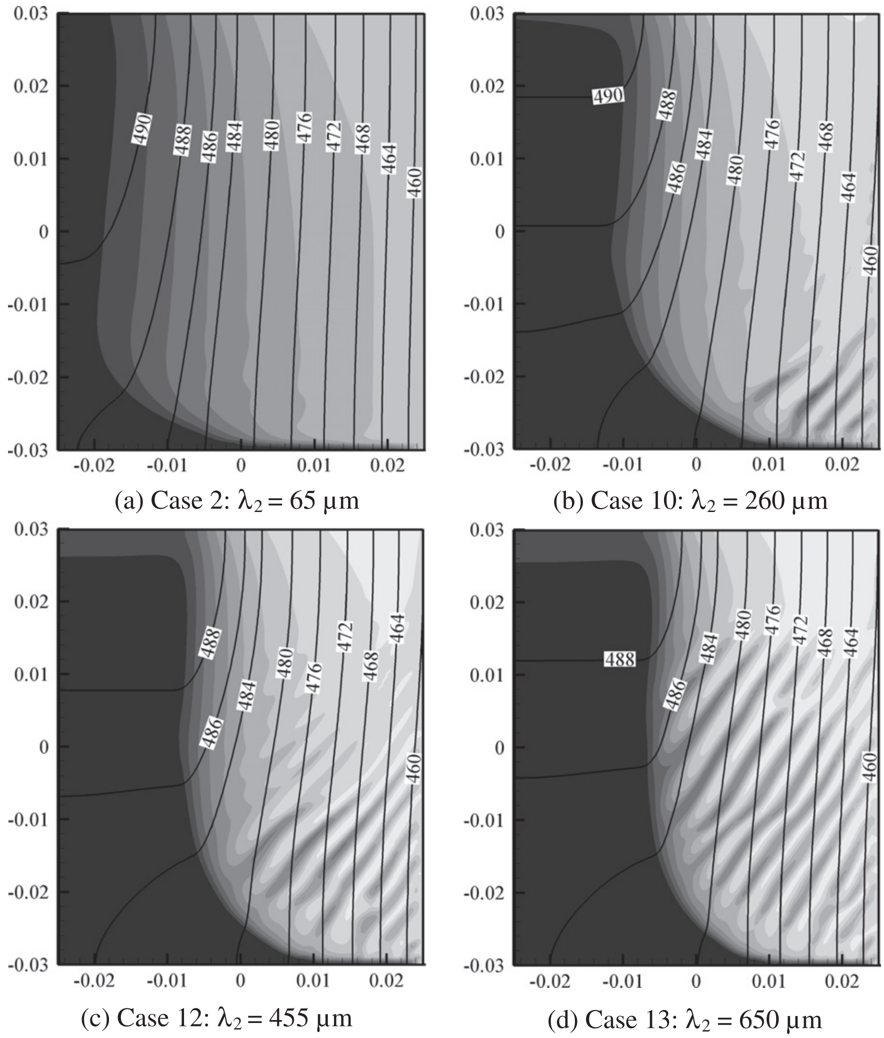

Fig. 7. Influence of λ_2 on f_ℓ and T at t = 150 s, where f_ℓ is shown in gray scale (dark for 1 and light for 0) and T is shown in isothermals. (a) Case 2: λ_2 = 65 μm; (b) Case 10: λ_2 = 260 μm; (c) Case 12: λ_2 = 455 μm; (d) Case 13: λ_2 = 650 μm.

to 260, 455, and 650 μm, the number of channels formed is 4, 7 and 11, respectively. The length of the channels is also influenced by λ_2. With a larger λ_2, the channels extend (penetrate) deeper into the mushy zone. For Case 13 (λ_2 = 650 μm) the channel segregation zone occupies more than half of the mold cavity. Based on these results, it can be concluded that a large Rayleigh number promotes channel formation.

Examining the global maximum c_{mix}, which occurs in the lower left (near the plane of symmetry), and the global minimum c_{mix}, which occurs in the upper right region near the casting surface, shows that the minimum c_{mix} and maximum c_{mix} are also strongly influenced by λ_2 (Fig. 9). Two situations spanning the range of λ_2 must be distinguished. Firstly, when λ_2 is small (<130 μm) when very few or no channels appear, the maximum c_{mix} increases while the minimum c_{mix} decreases with increasing λ_2. This is due to the significantly enhanced global flow in the mold cavity, caused by the increased permeability of the mushy zone. A stronger flow means enhanced transport of segregated interdendritic melt, hence stronger macrosegregation. Secondly, when λ_2 is large ($\geqslant$195 μm) and a greater number of channels appear, both maximum c_{mix} and minimum c_{mix} decrease with increasing λ_2. The reason for the decrease of the global maximum c_{mix} is due to the entrapment of the solute element by the segregation in the channels. The minimum c_{mix} occurs in the upper right region near the casting surface, an area less influenced by the channel formation. Therefore, the minimum c_{mix} continues to decrease with the enhanced global flow intensity in the mold cavity.

To further quantify channel segregation and characterize channel features the following parameters are defined: maximum channel length (l), channel space (δ), and channel inclination angle (θ), as schematically shown in Fig. 10. The severity of segregation across a channel is evaluated by a channel segregation severity index (Γ), defined as

$$\Gamma = \frac{c_{\mathrm{mix}}^{\max} - c_{\mathrm{mix}}^{\min}}{c_0} \times 100\%, \tag{8}$$

where $c_{\mathrm{mix}}^{\max}$ is the local maximum of c_{mix} within the channel, $c_{\mathrm{mix}}^{\min}$ is the local minimum of c_{mix} between two neighboring channels and c_0 is the nominal concentration. The local maximum and minimum concentrations used in Eq. (9) are distinguished from the global maximum and minimum concentrations discussed in the previous section. Determination of the segregation parameters (l, δ and θ) from the current simulation results, for instance in Fig. 8, is done by a visual measurement. The values of δ and θ are averaged for each simulation case. The current discussion serves only as qualitative evaluation of the dependency of the segregation parameters on λ_2.

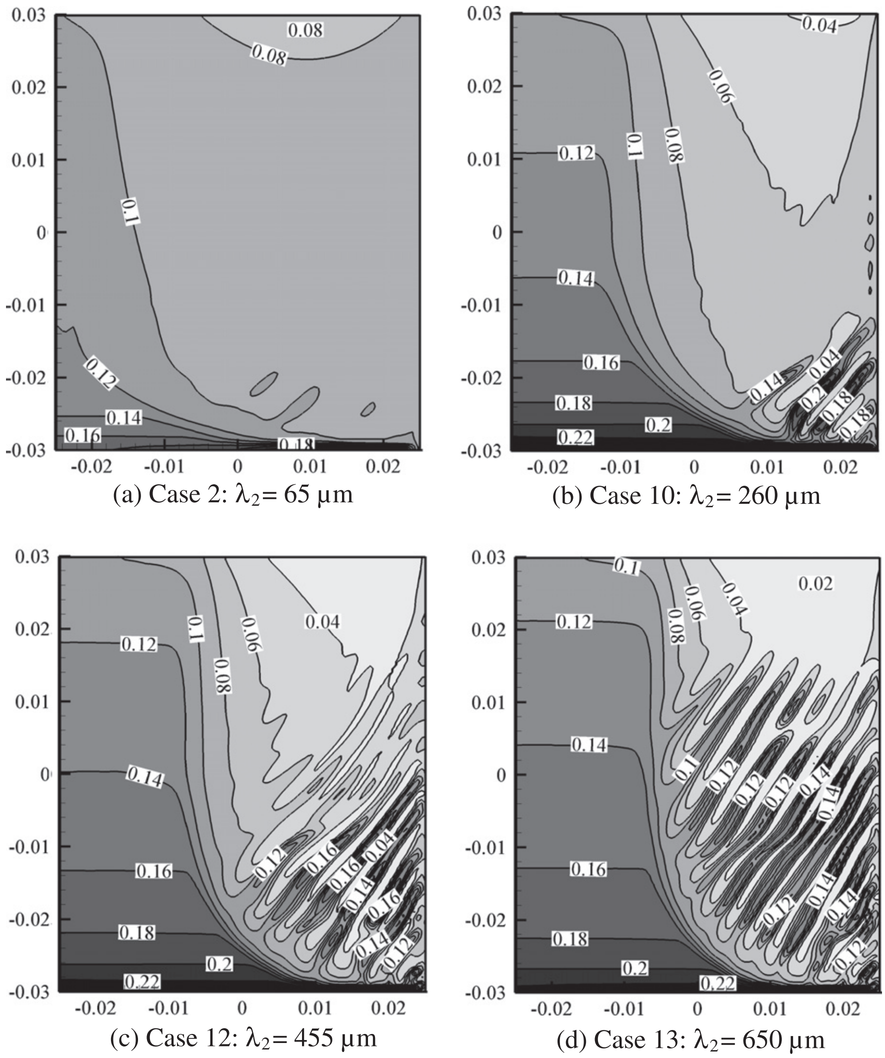

Fig. 8. Influence of λ_2 on c_{mix}, shown in gray scale and isolines (t = 150 s). (a) Case 2: λ_2 = 65 μm; (b) Case 10: λ_2 = 260 μm; (c) Case 12: λ_2 = 455 μm; (d) Case 13: λ_2 = 650 μm.

The influence of λ_2 on the above segregation parameters is shown in Figs. 11 and 12. The channel spacing, δ, decreases and the maximum channel length, l, increases with increasing λ_2. The channel inclination angle increases with increasing λ_2, while the channel segregation severity index, Γ, initially increases and then decreases. Thus, channel segregation tends to occur for the cases of large λ_2, but the severity of segregation is reduced with further increase of λ_2. Precise evaluation of the above dependencies is out of the scope of the current study and requires further investigations.

3.2. Local Rayleigh number

The local R_a number in the mushy zone (Eq. (1)) and its correlation to the formation of channel segregation are examined via

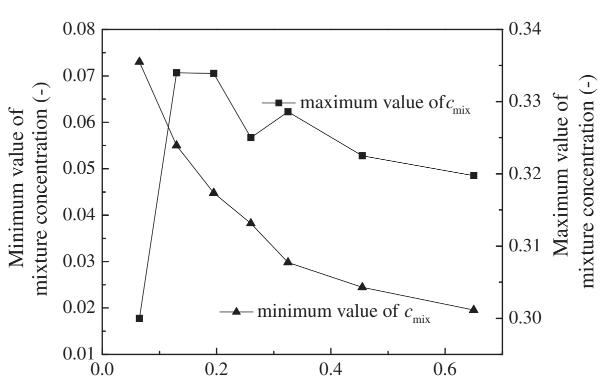

Fig. 9. The influence of λ_2 on the global maximum and the minimum value of mixture concentration (c_{mix}) in the computational domain.

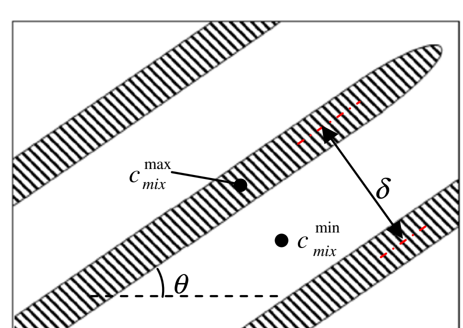

Fig. 10. Schematic definition of channel segregation parameters. The shaded regions indicate the channels.

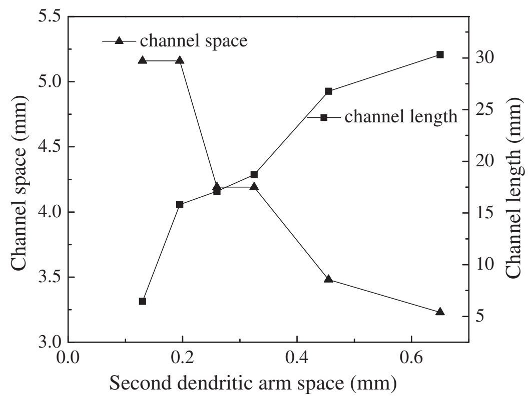

Fig. 11. Influence of λ_2 on channel spacing, δ, and maximum channel length, l.

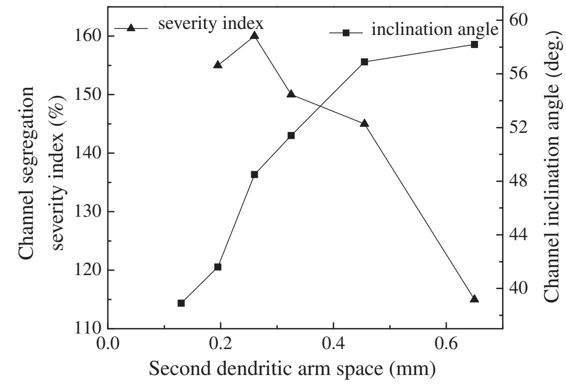

Fig. 12. Influence of λ_2 on channel inclination angle, θ, and channel segregation severity index, Γ.

Fig. 13. The h in Eq. (1) is estimated by $(T_{\text{liquidus}} - T)/G$, and the average permeability $\overline{K}$ is replaced by the local K. Distribution of the R_a number in the mushy zone is shown in Fig. 13. The R_a number initially increases in the mushy zone with increasing distance from the liquidus isotherm (h), reaching its maximum at a position very close to the solidification front (liquidus isotherm), where the solid fraction is about 0.03. As h further increases the R_a number decreases in the deep mushy zone, implying that the onset of flow instability may occur very close to the solidification front in the mushy zone. If there is any possibility for a channel to form, it will form in the front of the mushy zone. Upon initial channel forma-

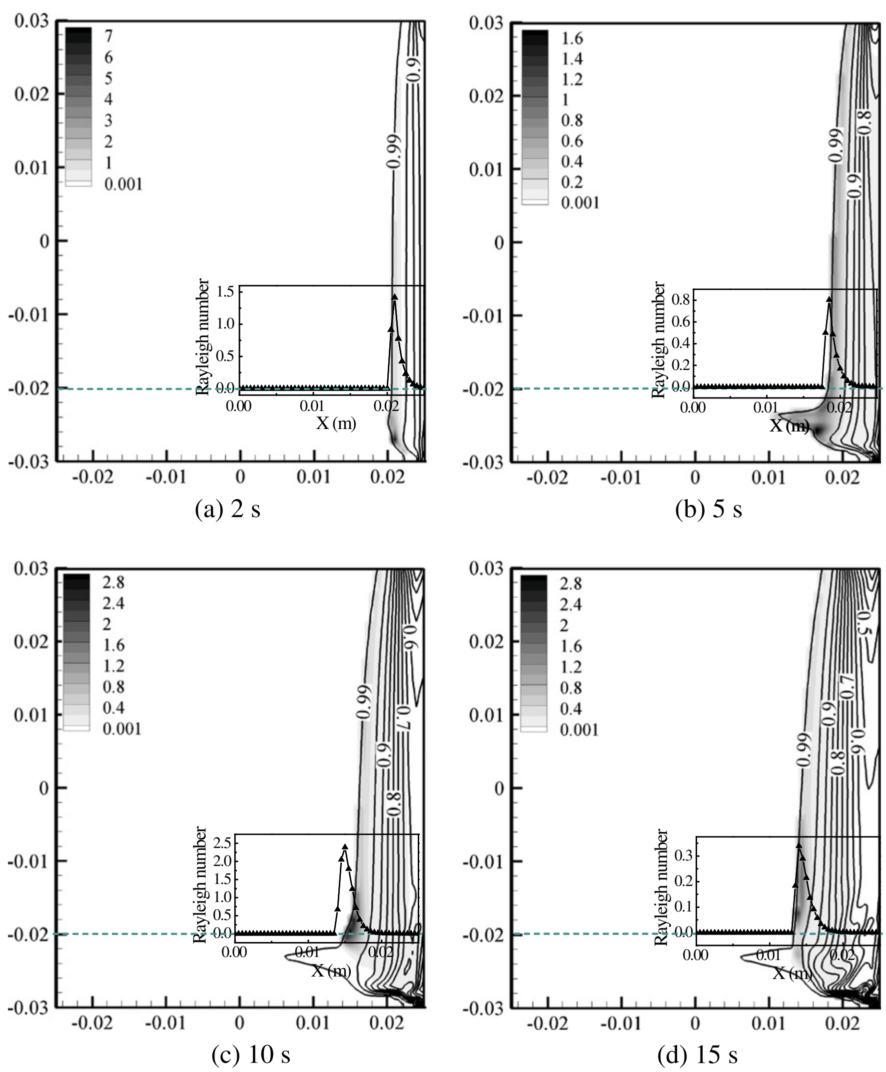

Fig. 13. R_a number distribution in the solidifying mushy zone: (a) at 2 s; (b) at 5 s; (c) at 10 s; (d) 15 s. The R_a number distribution is shown in gray scale, overlaid with the liquid volume fraction f_ℓ. The inserted diagrams show the R_a number distribution profiles along the marked horizontal lines. This simulation is performed with $\lambda_2 = 455$ μm.

tion, the channel continues to 'grow' via the flow-solidification interaction. This 'growth' does not occur by re-melting of the already-solidified phase, it is due to the change of the solidification rate in the immediate neighboring regions.

Uncertainty over a precise definition of a critical R_a number for channel formation has prevented us from using this criterion to predict channel formation directly. Table 1 summarizes the maximum Rayleigh number ($R_{a,Max}$) of each simulation case during initial stage of solidification. This $R_{a,Max}$ number can be used as an indicator to analyze the tendency of channel formation. The larger the $R_{a,Max}$, the more likely a channel will form. If $R_{a,Max}$ is correlated with the event of channel formation (yes or no), it is found that the cases with channel segregation must have a $R_{a,Max}$ larger than a critical value. This critical value is likely to fall in a range between 0.12 and 0.24, which is coincidently similar to the value as suggested by Beckermann and co-authors (0.25) [12], although here a different casting configuration and alloy are used. Normally, this critical number is dependent on the alloy even on the casting configuration.A more precise critical $R_{a,Max}$ number could be identified through additional studies of Case 4 and Case 5, however this would not be entirely straightforward. Case 4 without channels and Case 5 with clearly identified channels can only be visually distinguished-these differences cannot, under the current analysis, be quantitatively expressed. Secondly, the maximum $R_{a,Max}$ number recorded in Table 1 does not represent the value at the exact position and moment of channel formation. This value cannot be used as criterion to predict the position of the channel initialization. Additionally, as previously discussed (Section 2.1), the flow-solidification interaction plays a significant role in the channel formation as well. In the upper-right region of the benchmark where the flow-solidification interaction term $\vec{u}_\ell \cdot \nabla c_\ell$ is positive, a channel would not form even the critical $R_{a,Max}$ number is reached. Therefore, both the $R_{a,Max}$ number and the flow-solidification interaction term $\overline{u}_\ell \cdot \nabla c_\ell$ should be considered when analyzing the formation mechanism of the channel segregation.

4. Conclusions

In Part II of this two-part investigation the mechanism leading to the formation of channel segregation in a laterally solidified Sn–10 wt.% Pb benchmark was numerically studied. Both the initiation and growth of the channels were examined. The former is caused by flow perturbations in the mushy zone, which has been characterized by a mushy zone Rayleigh (R_a) number [6,7,12] and the latter is the result of flow-solidification interactions [4,5].

The parameter studies have verified the use of the R_a number as a qualitative indicator for initialization of channel segregation. The cases with high R_a number, obtained by increasing the secondary dendrite arm spacing λ_2 and the solutal expansion coefficient β_c, are prone to channel segregation. A further step is taken to correlate the maximum Rayleigh number ($R_{a,Max}$) with the event of channel formation. For cases with channel segregation $R_{a,Max}$ must be larger than a critical value, determined to be in a range between 0.12 and 0.24. Coincidently, this $R_{a,Max}$ is similar to the value as found by Beckermann and co-authors (0.25) [12]. The above critical value of $R_{a,Max}$ cannot be used for firm quantitative prediction of channel formation as it does not represent the value at the exact position and moment of channel formation. Further studies are needed to identify a well-defined critical $R_{a,Max}$.The R_a criterion alone is not a sufficient condition to predict channel segregation; the growth and stability of the channels must be determined by the resulting interdendritic flow-solidification interaction. With the assumption of the infinite solute diffusion in the interdendritic melt, Meherabian and co-authors proposed a flow-solidification interaction term, $\vec{u}_\ell \cdot \overline{G}$, to qualitatively analyze channel formation [1,4,5]. The justification of using this term when solute diffusivities in the interdendritic melt are large is verified by the current model. The reported numerical parameter studies have demonstrated the influence of solute diffusivity in channel formation. For low solute diffusivity, the definition of the flow-solidification interaction term $\overline{u}_\ell \cdot \nabla c_\ell$ should be used to avoid overestimation of channel segregation by the assumption of the infinite diffusion.

The sign of the flow-solidification interaction term, $\overline{u}_\ell \cdot \nabla c_\ell$, can be used to distinguish two solidification regions: a suppressed solidification region, where the sign of the flow-solidification interaction term is negative (flow is in the opposite direction of the liquid concentration gradient); and an accelerated solidification region, where the sign of the flow-solidification interaction term is positive (flow is in the same direction of the liquid concentration gradient). Channels can only occur in the suppressed solidification region, where an increase in local flow caused by a flow perturbation is reinforced by the resulting suppressed solidification. In this situation the flow becomes unstable and channels continue to grow. Channels do not form in the accelerated solidification region, where an increase in local flow intensity due to a flow perturbation is throttled by the resulting accelerated solidification. In this latter case flow perturbation is stabilized by flow-solidification interactions.

In the current benchmark simulation, remelting does not occur during channel formation, indicating that remelting is not a necessary condition for channel formation, which confirms a recent finding of Sawada et al. [22].

Acknowledgments

The authors acknowledge the discussions of the modeling results with Prof. H. Combeau from CNRS-Nancy and Prof. Y. Fautrelle from CNRS-SIMAP-EPM, France. The financial support by the Austrian Federal Ministry of Economy, Family and Youth and the National Foundation for Research, Technology and Development is gratefully acknowledged. Jun Li would like to thank the support from the China Scholarship Council.

References

[1] M.C. Flemings, G.E. Nereo, Trans. TMS-AIME 239 (1967) 1449–1461.
[2] R.J. McDonald, J.D. Hunt, Trans. TMS-AIME 245 (1969) 1993–1997.
[3] A. Kumar, B. Dussoubs, M. Založnik, H. Combeau, J. Phys. D: Appl. Phys. 42 (2009) 105503–105515.
[4] R. Meherabian, M. Keane, M.C. Flemings, Metall. Trans. 1 (1970) 1209–1220.
[5] J.J. Moore, N.A. Shah, Inter. Metals Rev. 28 (1983) 338–356.
[6] A.K. Sample, A. Hellawell, Metall. Trans. A 15 (1984) 2163–2173.
[7] M.G. Worster, Ann. Rev. Fluid Mech. 1 (1997) 91–122.
[8] K. Suzuki, T. Miyamoto, Trans. Iron Steel Inst. Jpn 14 (1974) 296–305.
[9] K. Suzuki, T. Miyamoto, Trans. Iron Steel Inst. Jpn 18 (1978) 80–89.
[10] W.H. Yang, J.J. deBarbadillo, K. Morita, T. Suzuki, W. Chen, K.M. Chang, JOM 56 (2004) 56–61.
[11] S.M. Copley, A.F. Giamei, S.M. Johnson, M.F. Hornbecker, Metall. Trans. 15A (1970) 2163–2173.
[12] C. Beckermann, J.P. Gu, W.J. Boettinger, Metall. Mater. Trans. A 31 (2000) 2545–2565.
[13] T. Sawada, K. Oikawa, K. Anzai, in: S.L. Cockroft, D.M. Maijer, (Eds.), Modeling of Casting, Welding and Advanced Solidification Processes XII, TMS, Warrendale, PA, USA, 2009, pp. 303–310.
[14] G. Guillemont, C. Gandin, M. Bellet, J. Crystal. Growth 303 (2007) 58–68.
[15] M. Medina, Y.D. Terrail, F. Durand, Y. Fautrelle, Metall. Mater. Trans. B 35 (2004) 743–754.
[16] J. Guo, C. Beckermann, Numer. Heat Tr. A-Appl. 44 (2003) 559–576.
[17] E. Yoshio, Metall. Mater. Trans. B 42 (2011) 341–369.
[18] T.M. Pollack, W.H. Murphy, Metall. Mater. Trans. A 27 (1996) 1081–1094.
[19] M. Wu, A. Ludwig, Metall. Mater. Trans. A 37 (2006) 1613–1631.
[20] M. Wu, A. Ludwig, Metall. Mater. Trans. A 38 (2007) 1465–1475.
[21] M. Wu, L. Könözsy, A. Ludwig, W. Schützenhöfer, R. Tanzer, Steel Res. Int. 79 (2008) 56–63.
[22] T. Sawada, K. Oikawa, K. Anzai, F. Takahashi, K. Kajikawa, H. Yamada, J. JFS 82 (2010) 142–148.